Journal of
Engineering Sciences
Faculty of Engineering
Assiut University
JES
مجلة
العلوم الهندسية
كلية الهندسة
جامعة أسيوط
journal homepage: http://jesaun.journals.ekb.eg

Comparison of Different Approaches for Combining Gravity Field Wavelengths for Egypt

Received 4 November 2023; Revised 23 December 2023; Accepted 23 December 2023

Hussein A. Abd-Elmotaal [1]
Mostafa Ashry [2]
Atef Makhloof[3]

Keywords
Remove- restore technique; GPS-levelling; Heck geoid; Meissl Geoid; Gore geoid,

Abstract
Within the context of the remove-restore technique, this research seeks to determine the best combination of gravity field wavelengths for Egypt's geoid computation. There are various methods for such a wavelength combination. It has been proposed to merge the regional data signals and the global geopotential earth models, potentially using a modified Stokes' kernel with various methods. The double consideration of the topographical and compensating masses within the computed window has been properly addressed by a technique called the window approach. Within the framework of the geoid computation, a thorough comparison of the modified Stokes' kernel with different approaches and window techniques has been conducted. The comparison is made at two separate levels: the gravity anomalies after reduction to geoid following the correct removal step and the determined geoid heights concerning the geoid determined from GPS-levelling (GPS-GEOID). Firstly, from our computations, it can be concluded that the conventional remove-restore technique should not be applied for the determination of gravity anomalies and geoid determination. Also, the outcomes demonstrated that the estimated gravity anomalies utilizing the window approach are independent, the finest, and unbiased and have a minimal difference between the maximum and minimum values. The geoid produced from the GPS levelling has fewer differences between it and the geoids computed using the modified Stokes' kernels as well as the geoid determined using the window technique than in the case of utilizing the unmodified Stokes' classical kernel. Finally, the window approach gives, however, completely better outcomes compared to the Stokes unmodified kernel method.

1. Introduction

The precise determination of local geoids is very important for engineering and surveying applications and as a reference surface, e.g., for hydrological and oceanographic studies. On the

[1] Professor, Civil Engineering Dept., Faculty of engineering, Minia University, Minia, Egypt. Hussein.abdelmotaal@gmail.com
[2] Lecturer, Civil Engineering Dept., Faculty of engineering, Minia University, Minia, Egypt mostafa.ashry@mu.edu.eg
[3] Assoc. Prof., Civil Engineering Dept., Faculty of engineering, Minia University, Minia, Egypt atefmakhloof@yahoo.com

https://doi.org/ 10.21608/JESAUN.2023.246329.1283

other hand, the knowledge of the Earth's gravity field in the form of gravity anomalies is important to geophysics.

The geophysical applications of geoid cover: the upper crust density anomalies, deep earth mass anomaly structure, strain and stress field, oceanic lithosphere structure, rotation of the earth geophysical prospecting. Many methods for geoid determination are time-independent. To investigate the causes of the variations is of great interest to geophysicists, seismologists, and oceanographers. Therefore, not only the geoid but also its variation needs to be precisely determined. Overall, a wide range of geodetic, precise engineering, geophysical, and oceanographic applications render a need for precise geoid estimation and its variation with time. Although the precision of the geoid has been greatly improved in recent decades, it still does not offer sufficient accuracy for some applications [1].

The spherical geodetic boundary-value problem must be solved for the gravimetric determination of the geoid to be estimated, and Stokes's convoluting integral surface must be evaluated. In reality, satellites and terrain gravity data are merged to estimate the gravimetric geoid. The method used in this contribution is to separate the geoid undulations into low-frequency reference field, which is calculated using a spherical harmonic gravitational model acquired from satellite data, and the high-frequency geoid, which is calculated from terrain gravity data. The numerical evaluation of the Stokes formula with an adaptation is necessary due to the high-frequency ingredient of the geoid in the source gravitational data set. Generally, discrete numerical integration can be used to find the solution (i.e., quadrature-based summation). As an alternative, the boundary problems can be resolved by combining the frequency domain spectra of Stokes's function and gravity data with Stokes' convolution integral from the space domain [2].

Numerous authors have investigated the ideal combination of gravity-field wavelengths within the geoid computation framework for various earthly areas. This research seeks to determine which method provides the optimum merging of gravity field wavelengths for determining Egypt's geoid. For more information, it is referred to, e.g., [3-13]

This study presents a comparison of five methods: the classical unmodified Stokes' kernel, the Meissl's modified kernel; the Wong and Gore modified kernel, the Heck and Grüninger modified kernel; and the window remove-restore technique for calculating Stokes' integral.

The available gravity data, GPS data, and Digital Terrain Models (DTMs) for this study are given. The GO CONS GCF 2 TIM R3 [14] geopotential model is applied in current research. It has been turned out that, GO CONS GCF 2 TIM R3 had a good performance when validated with gravity data in Egypt [16]. Utilizing the remove-restore approach with both unaltered and modulated Stokes' kernels, the Stokes' integral for computing the geoid is outlined in more detail in the ensuing subsections. The study also outlines the window-remove-restore approach introduced by [18]. Consequently, T/I potential harmonic analysis is then provided. Both the conventional remove-restore and the window remove-restore procedures are applied to reproduce and compare the reduced-gravity anomalies. The gravimetric geoids for Egypt have been generated by employing the five alternate methodologies that were taken into consideration for the current inquiry. These approaches have been thoroughly compared within the domain of geoid determination.

Journal of
Engineering Sciences
Faculty of Engineering
Assiut University
JES
مجلة
العلوم الهندسية
كلية الهندسة
جامعة أسيوط
journal homepage: http://jesaun.journals.ekb.eg

2. The Data considered for the current study.

2.1 Gravity in sea and land for Egypt

Figure 1-a demonstrates the gravity stations that are currently available for our investigation. Large gaps and uneven distribution, particularly on land, are shown in Fig. 1. The authors have been gathering data on land gravity from various sources for the past 20 years. The Bureau Gravimétrique International (BGI) has made available a set of shipborne gravity data for the sea. According to [15], a gross-error detection technique has been implemented. The gravity data for Egypt are extended form ($19^{\circ}N \leq \phi \leq 35^{\circ}N$ in latitude and $22^{\circ}E \leq \lambda \leq 40^{\circ}E$ in longitude). The Red Sea's data point distribution is more evenly distributed than the Mediterranean Sea's. The total count of the gravity stations is 102,418. The free-air gravity anomalies for Egypt are shown in Fig, 1-b The maximum and minimum values of free-air anomalies for Egypt are −210.6 and 315.0 mGal, respectively, and 27.58 mGal on average, with a standard deviation of roughly 50.65 mGal.

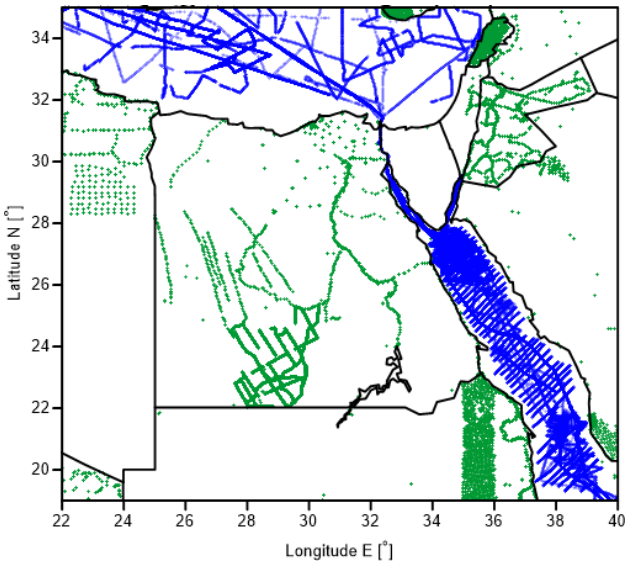

Figure 1-a Measurement Stations of gravity in both sea and land areas all over Egypt

2.2. GPS Benchmarks

Figure 2 demonstrates the existing GPS nodes that have orthometric heights, which are applied to determine the differences between the geoid estimated from GPS and the different computed gravimetric geoids presented in the current study. Due to the lack of GNSS-levelling-based geoid, GPS data were employed in this investigation. Also, The GPS points refer to the High Accuracy Reference Network (HARN) of Egypt. Thirty GPS stations are present overall, which is insufficient for Egypt's surface area. The GPS-GEOID heights for the points in Egypt range between 7.3 and 21.5 meters. The GPS stations are distributed quite uniformly.

https://doi.org/ 10.21608/JESAUN.2023.246329.1283

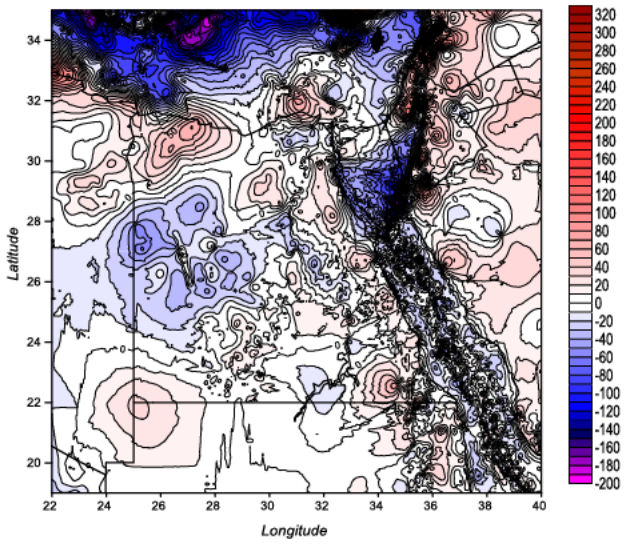

Figure 1-b Free-air gravity anomalies for Egypt. [Units in [mgal].

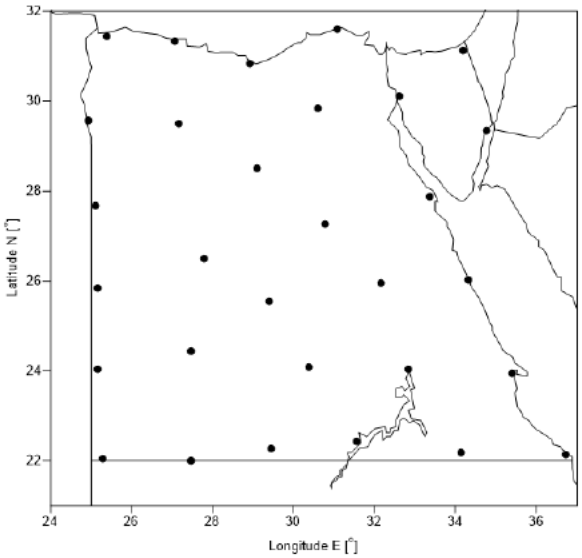

Figure 2 Accessible GPS locations with orthometric height observations.

2. 3. Digital Terrain Models

For computing terrain effects, a collection of coarse and fine DTMs is required. For this inquiry, the coarse DTM EGH13S30 30″ × 30″ [17] and fine DTM EGH13S03 3″ × 3″ [19] are both accessible. These digital terrain models are extended form ($19^{\circ}N \leq \phi \leq 35^{\circ}N$ in latitude and $22^{\circ}E \leq \lambda \leq 40^{\circ}E$ in longitude); see, Fig. 3. These (DTMs) have been validated using the point reference validation data that is currently available for both land and ocean. On land regions, there are around 200 thousand points accessible for point reference-checking, whereas there are over one million points available for point reference-checking on the ocean. In Both regions, the differences fully fit the Gaussian normal distribution. Most discrepancies are under 20 meters on land and under 2 meters in ocean [19].

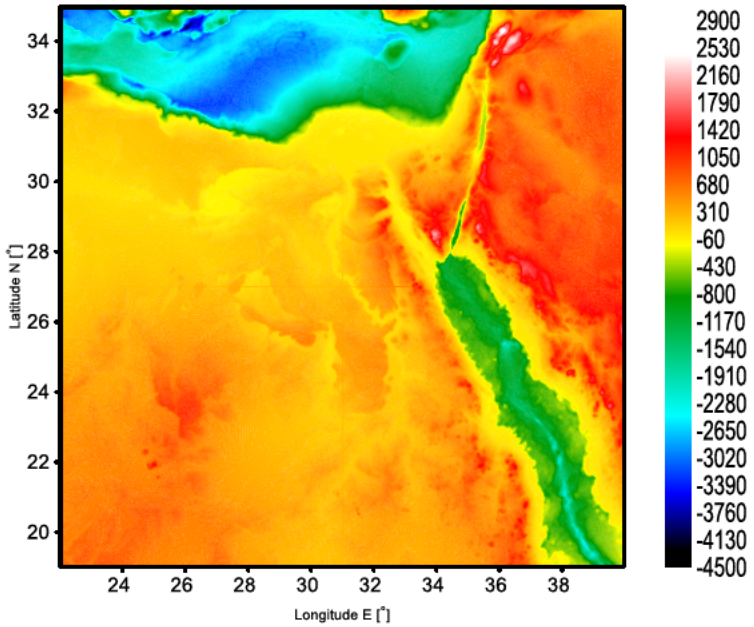

Figure 3 The fine 3″ × 3″ DTM (EGH13S03), after [19]. Units in [m].

3. Conventional Remove-Restore Method (RRM)

The RRM includes two separate proceedings: removal and restoration processes. In the removing step, the impacts of topography and its compensating masses and the impacts of the global reference model are eliminated from the original gravitational data (free-air anomalies) to give the reduced anomalies at the geoid. The topographic and its compensating masses and global geopotential model influences are added to the generated geoidal undulations in the restore step. The gravity/anomalies after applying the removing step in the RRM are estimated by (see, e.g., [20-23]).

$$\Delta g_{red} = \Delta g_F - \Delta g_{GM} - \Delta g_h \quad \textbf{(1)}$$

where indicates the differences between the gravity on the geoid and the normal gravity refers to the reference ellipsoid (denotes the free-air anomalies), denotes the impact of the Topographic/Isostatic (T/I) masses, and denotes the impact of the gravitational reference field. Consequently, the final estimated geoid heights N are given by:

$$N = N_{\Delta g_{red}} + N_{GM} + N_{TI} \quad \textbf{(2)}$$

where represents the geopotential gravity field contribution, represents reduced anomalies' impact, and is the effect of T/I masses.

4. Stokes' Classical Kernel used in Stokes' Integral

A solution to the geodetic boundary value issue was introduced by G.G. Stokes in 1894, where the geoid undulation N can be calculated through a global coverage of gravity anomalies all over the entire Earth. The geoid heights resulting from the reduced gravity anomalies are determined by the Stokes' integral [24].

$$N_{\Delta g} = \frac{R}{4\pi\gamma}\iint_{\sigma} \Delta g_{red} S(\psi)\, d\sigma \qquad \textbf{(3)}$$

where R represents the mean radius of the Earth, γ stands for the normal gravity of the reference ellipsoid, dσ is the surface element of integration over the unit sphere, and S(ψ) stands for the original Stokes function and can be presented in closed form:

$$S(\psi) = \frac{1}{s} - 4 - 6s + 10s^2 - (3 - 6s^2)\ln(s + s^2) \qquad \textbf{(4)}$$

with and the geocentric angle ψ is the spherical distance measured on the sphere with radius R between the radius vectors of the computation point P and the integration point Q. Numerical integration is used to determine the integral in Eq. (3)); consequently, it is transformed to:

$$N(\varphi_P, \lambda_P) = \frac{R\Delta\varphi\Delta\lambda}{4\pi\gamma}\sum_{Q}(\Delta g_Q \cos\varphi_Q) s(\psi_{PQ}) \qquad \textbf{(5)}$$

As previously discussed, in the remove-restore-technique, the Stokes approach with kernels regarding to original Stokes cannot properly manage the merging of the various wavelengths for the gravitational field of the Earth. To address this issue, the Stokes kernel can be amended as a potential remedy. In the following, different modified Stokes' kernels will be summarized.

5 .Modified Stokes Kernel

The surface integral in Stokes' formula must be applied to the entire Earth. However, due to the restricted availability of gravity anomaly data, the area is practically constrained to a limited spherical distance surrounding the point under consecration. Therefore, the surface integral cannot be applied to the global surface of the Earth. Therefore, the Stokes function must be modified, as illustrated in [25]. In the following sections, different modified Stokes kernels will be studied.

5.1 Meissl Modification

The kernel is modified in this approach by simple subtraction. Thus, the geoid height can be calculated as:

$$N = \frac{R}{4\pi\gamma}\iint_{\sigma} \Delta g_{red} S^{ME}(\psi)\, d\sigma \qquad \textbf{(6)}$$

where represents Meissl-modified-kernel and is given by [26] as follows:

$$S^{ME}(\psi)=\begin{cases} S(\psi)-S(\psi_0) & for\ 0\le\psi\le\psi_0 \\ 0 & for\ \psi_0\le\psi\le\pi. \end{cases} \quad (7)$$

The geoid estimated from GPS-levelling and the calculated geoids are contrasted to empirically determine the ideal cap size ψ◦ (capsize ψ◦). Meissl demonstrates that the truncation error series converges to zero more quickly by exceeding the spherical harmonic degree n. Therefore, compared to a kernel that has not been modified, the impact of truncation error on the geoid is reduced at a faster rate. This is due to the fact that a continuous kernel function's Fourier coefficients reach zero faster than a discontinuous one's.

5.2 Wong and Gore Modification

The original Stokes was modified by [27] by eliminating the low-degree terms of the Legendre-polynomials from the original Stokes function. The Fourier series of Legendre-polynomials from 2 to infinity can be used to express the classical unmodified Stokes kernel, as shown in the following example by [28] as follows:

$$\mathrm{S}(\psi)=\sum_{n=2}^{L}\frac{2n+1}{n-1}P_k(\cos\psi) \quad \textbf{(8)}$$

The low-degree terms in Stokes' integral from 2 to L, inclusive, can be removed from the integral in Eq. (3) due to the orthogonality of spherical harmonics on the sphere when a global geopotential model of spherical harmonic degree and order L is included [24,26]. The Wong and Gore kernel takes the form [26] as follows:

$$S^{L}(\psi)=\mathrm{S}(\psi)-\sum_{n=2}^{L}\frac{2n+1}{n-1}P_k(\cos\psi) \quad \textbf{(9)}$$

In the process of computing the truncation error, the degree of modification L, which corresponds to the capsize ψ◦, is computed according to [27] as follows:

1. Select L value.
2. For the selected L, take into account the modified Stokes kernel function.
3. Find the initial zero of SL(ψ) iteratively in Eq. (9) to get the capizeψ◦ corresponding to the selected L.

Again, to empirically establish the optimal capsize ψ◦ the geoid estimated from GPS-levelling and the gravimetrically determined geoid undulations are compared.

5.2.1 The Truncation Error

The calculation of geoidal height N is computed from Stokes' formula as follows

$$N=\frac{R}{4\pi\gamma}\int_0^{2\pi}da\int_0^{\pi}[\ \Delta\mathrm{g}(\mathrm{a},\psi)\mathrm{S}(\cos\psi)sin\psi\ ]d\psi \quad \textbf{(10)}$$

where) is the Stokes' function given by Eq. (4). The numerical integration in the previous equation is often performed up to a selected angular distance ψ◦ around the computing point in practice. As a result, a truncation error happens in the geoidal height, which is determined by:

$$\delta N = \frac{R}{4\pi\gamma}\int_0^{2\pi} da \int_{\psi o}^{\pi} \Delta g(a,\psi) S(\cos\psi) \sin\psi \, d\psi \qquad \textbf{(11)}$$

The harmonic analysis of this truncation error is found in [25]:

$$\delta N = \frac{R}{2G}\sum_{n=2}^{\infty} Q_n(\cos\psi o)\Delta g_n \,, \qquad \textbf{(12)}$$

with

$$Q_n(\cos\psi o) = \int_{\psi o}^{\pi} S(\cos\psi) P_n(\cos\psi)\sin\psi \, d\psi, \,, \qquad \textbf{(13)}$$

where stands for the order zonal harmonic component of Δg at the point under consecration and represents the Legendre-polynomial of degree n. More detailed information and explicit expressions can be found in [29]. Expanding the gravity anomaly into its harmonic coefficients is performed by employing a harmonic analysis technique. Many authors have developed various harmonic analysis techniques. The reader is invited to refer to, e.g., [31] for a harmonic analysis technique on the surface of the sphere or [32] and [33] for harmonic analysis techniques on the sphere.

5.3 Modification according to Heck and Grüninger

Heck and Grüninger [34] proposed an amendment similar to that introduced by Meissl; however, in this case, the subtraction is implemented with the spheroidal kernel. This modification) can be formulated as [11]:

$$S^{HG}(\psi) = \begin{cases} S^k(\psi) - S^k(\psi_0) & \text{for } 0 \le \psi \le \psi_0 \\ 0 & \text{for } \psi_0 \le \psi \le \pi. \end{cases} \qquad \textbf{(14)}$$

with

$$S^k(\psi) = S(\psi) - \sum_{n=2}^{k} \frac{2n+1}{n-1} P_k(\cos\psi) \qquad \textbf{(15)}$$

and

$$S^k(\psi_0) = S(\psi_0) - \sum_{n=2}^{k} \frac{2n+1}{n-1} P_n(\cos\psi_0) \qquad \textbf{(16)}$$

When the Heck-Gru¨ninger modified kernel is used with the removed-restore approach, it lessens the truncation error [11]. According to [28,35,36], the degree of modulation k often extended from 2 to 360.

In evaluating the degree of modification k, corresponding to the capsize ψ◦, one may use the following procedure [30]:

1. Select a value for k
2. For the selected k, take into account the updated Stokes kernel relation.
3. Find the first minimum of SHG (ψ) iteratively in Eq. (14) to get the capize ψ◦ corresponding to the selected k.

Again, to empirically determine the optimal capsize ψ◦, the geoid determined using GPS and the gravimetrically determined geoids are analyzed and compared.

6. The Window Remove-Restore Method (WRRM)

To address the issue of part of the T/I masses near the computational point being considered twice, Abd-Elmotaal and Ku¨htreiber [18] proposed this technique. This approach offers an efficient method for creating preferable combinations of the gravitational field wavelength.

The influence of the T/I masses inside the conventional RRM on potential and its derivatives is shown in Fig.4. The T/I masses inside the circle are used to calculate the impact of the local T/I masses (representing the short-wavelength ingredients) for a point P. Typically, the global reference field includes the T/I masses across the globe. Then, eliminating the reference field (which represents the long-wavelength ingredients), amendment of the effect of the global T/I masses is also eliminated, which is depicted as a rectangle in Fig. 4.

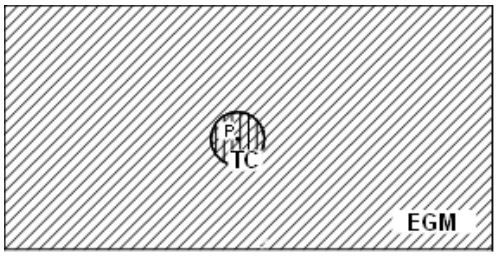

Figure 4 The conventional remove-restore method.

Abd-Elmotaal and Ku¨htreiber [18] introduced a solution to this issue by adapting the employed reference field according to the influence of the T/I masses for a specific data frame. The benefit of the WRRM is shown in Fig. 5. Utilizing the masses of the entire data window, the influence of the local T/I masses for point P under confederation is calculated (small rectangle). To produce the modified reference field, the influence of the T/I masses of the data window is subtracted from the reference field coefficients. Therefore, eliminating the component with a long wavelength utilizing this modified reference field prevents a portion of the T/I masses from being twice taken into account (there is not a double-hatched area in Fig. 5).

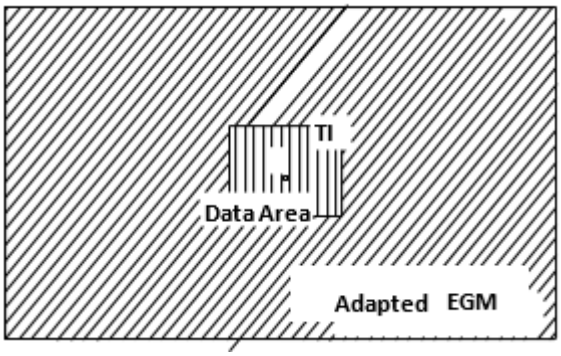

Figure 5 The window remove-restore technique.

The removal step of this technique is given by:

$$\Delta g_{win-red} = \Delta g_F - \Delta g_{GMAdapt} - \Delta g_{TIwin} \qquad \textbf{(17)}$$

where $\Delta g_{win-red}$ represents the gravity anomalies reduced by utilizing the window approach, $\Delta g_{GMAdapt}$ refers to the reference field's contribution after removing the spherical-harmonic-coefficients of the topography and its compensating masses, and Δg_{TIwin} represents the effect of the T/I masses within the constant data window. Then, the geoidal heights of this technique can be computed from

$$N_{\Delta g_{win-red}} = N_{GM\ Adapt} + N_{\Delta g} + N_{TIwin}\ , \qquad \textbf{(18)}$$

where $N_{\Delta g_{win-red}}$ stands for the effect of the window-reduced gravity anomalies on the geoid, $N_{GM\ Adapt}$ and N_{TIwin} represents the contribution of the adapted reference field, and *T/I* masses of the constant (fixed) data window (the indirect effect), respectively. It is worth pointing out that the influence of the gravity anomalies after reduction Δg_{win}-*red*, determined by Eq. (17), on the geoid $N_{\Delta g_{win-red}}$ is calculated by numerical integration of the original Stokes' kernel provided by Eq. (4).

7. Potential Spherical Harmonic of Topographic/Isostatic (T/I) Masses

The potential coefficients of the T/I masses $\bar{T}_{nm}$ and its harmonic series expansion T_{TI} (P) introduced by [18,37], are expressed as follows:

$$T_{TI}(p) = \frac{GM}{r_P}\sum_{n=0}^{\infty}\left(\frac{R}{r_P}\right)^n \sum_{m=-n}^{n}\bar{T}_{nm}\bar{R}_{nm}(P) \qquad \textbf{(19)}$$

Here $\bar{R}_{nm}(P)$ is identified by [21] as follows:

$$\bar{R}_{nm}(P)=\bar{P}_{nm}(\cos\theta_p)\begin{cases}\cos\lambda_P & for \quad n\geq 0\\ \sin\lambda_P & for \quad n\,\mathrm{p}\ 0\end{cases} \text{ - } \tag{20}$$

$\bar{P}_{nm}(\cos\theta_p)$ refer to the fully-normalized-Legendre-functions, GM represents the Newtonian constant of gravitational, r_P is the radius of the point under consideration and $\bar{T}_{nm}$ is given by

$$\bar{T}_{nm}=\frac{R^3}{M(2n+1)(n+3)}\iint\left\{\delta\rho_Q\left[\left(1+\frac{H_Q}{R}\right)^{n+3}-1\right]\right. \\ \left.+\delta\rho_Q\left(1-\frac{T_o}{R}\right)^{n+3}\left[\left(1-\frac{T_Q}{R-T_o}\right)^{n+3}-1\right]\right\}*\bar{R}_{nm}(Q)\,d\sigma_Q \tag{21}$$

In this relation, H denotes the topographic height, $T_\circ$ is the crustal thickness according to Airy, t is the compensating root/antiroot, and M refers to the Earth's mass, which can be calculated as:

$$M=\frac{4\pi R^3}{3}\rho_M\,, \tag{22}$$

ρ_M represents the mean density of the Earth [38], $\rho_M = 5.517$ g/cm^3.

To determine the potential spherical harmonic coefficients (SHC) of the T/I masses practically, the integration is replaced by a summation. Accordingly, Eq. (21) can be transformed to:

$$\bar{T}_{nm}=\frac{3\Delta\varnothing\Delta\lambda}{4\pi\rho_M(2n+1)(n+3)}\sum_i^{\phi}\sum_j^{\lambda}\left\{\rho_{ij}\left[\left(1+\frac{H_{ij}}{R}\right)^{n+3}-1\right]\right. \\ \left.+\Delta\rho_{ij}\left(1-\frac{T_o}{R}\right)^{n+3}\left[\left(1-\frac{t_{ij}}{R-T_o}\right)^{n+3}-1\right]\right\}*\left\{\begin{matrix}\cos m\lambda_j\\ \sin m\lambda_j\end{matrix}\right\}p_{nm}(\cos\theta_i)\cos\phi_i, \tag{23}$$

In the previous equation, the integral in the previous equation is replaced by latitude (ϕ) and longitude (λ). The grid spacing $\Delta\phi$ and $\Delta\lambda$ denote the size of the integration element in the latitude and longitude direction of the available DTM, respectively, and the density ρ is given by:

$$\rho=\begin{cases}\rho_0 & for \quad H\geq 0\\ \rho_0-\rho_w & for \quad H\,\mathrm{p}\ 0\end{cases} \tag{24}$$

where $\rho_0\ \rho_w and$ refer to the topographic density and the water density in ocean areas respectively. The density differences $\Delta\rho$ are determined by:

$$\Delta\rho=\rho_1-\rho_2\,. \tag{25}$$

In the case of using Airy's floating theory [24], the thickness of root/anti-root t under a mountain or ocean column is evaluated by implementing the principle of hydrostatic equilibrium, which is expressed in the spherical formulation [39]:

$$\rho_0 R^3\left[\left(1+\frac{H}{R}\right)^3-1\right]=\left(\rho_1-\rho_0\right)\left(R-T_0\right)^3\left[1-\left(1-\frac{t}{R-T_0}\right)^3\right] \qquad \textbf{(26)}$$

Regarding the root/antiroot thickness, this condition is rearranged as

$$\frac{t}{R-T_0}=1-\left\{1-\frac{\rho}{\rho_1-\rho}\left(1-\frac{T_0}{R}\right)^{-3}\times\left(1+\frac{H}{R}\right)^3-1\right\}^{\frac{1}{3}} \quad , \qquad \textbf{(27)}$$

where ρ is given by Eq. (24).

8. Gravity Reductions

For the current investigation, the geoid determination process and the gravity reduction have been carried out using the following set of parameters. These parameters have (practically) shown to provide the ideal outcome for Egypt (*cf.*, [40,41]).

$$\begin{aligned} T_0 &= 30km \\ \rho_0 &= 2.67\, g/cm^3 \\ \Delta &= 0.4 g/cm^3 \end{aligned} \quad . \qquad \textbf{(28)}$$

For the conventional RRM, GO CONS GCF 2 TIM R3, a gravitational model from order 0 up to degree and order of 250, has been implemented. This model has been chosen because it turned out to work suitably with the Egyptian gravity field up to degree and order 250 [42]. By deducting the potential (SHC) of the T/I masses for the area extended from ($19^\circ N \le \phi \le 35^\circ N$ in latitude and $22^\circ E \le \lambda \le 40^\circ E$) in longitude determined by Eq. (23) using the GO CONS GCF 2 TIM R3 coefficients, the adapted reference field has been generated. Then, the adapting reference field has been utilized for the WRRM.

The statistics for gravity reduction for the conventional and window remove-restore approaches are presented in Table 1. It is worth pointing out that the reduced anomalies for Stokes' integral with the modified Stokes' kernels are identical to those for the Stokes' kernel with the original (unaltered) Stokes' integral (denoted by Δg_{Airy} in Table 1).

Table 1 demonstrates that utilizing the window approach leads to the best-reduced anomalies (denoted by $\Delta g_{Airywin}$ in Table 1). The standard deviation has decreased by about a fourth while the range has dropped by approximately 10%. Additionally, the window-reduced anomalies are more accurately centered (less biased). Thus, the anomalies are reduced by utilizing the window approach, which is appropriate for geodetic and geophysical applications.

Table 1: Statistics of the reduced-gravity anomalies. Units in [mGal]

Reduced gravity	Min	Max	Mean	Sdv
Δg_{obs}	-210.6	315.0	-27.6	50.6
$\Delta g_{obs} - \Delta g_{GM} - \Delta g_{Airy'}$	-96.7	138.0	14.7	27.4
$\Delta g_{obs} - \Delta g_{GM\ Adapt} - \Delta g_{Airy\ Win}$	-93.7	117.3	-4.8	21.3

9. Geoid determination

To calculate the gravimetric geoids for Egypt, the gravity anomalies either affect the geoid heights $N_{\Delta g}$ $N_{\Delta g_{win-red}}$ or have been numerically computed. The geoid has been established using the several ways outlined in Sections 4, 5, and 6. These methods include Stokes' integral using the conventional original Stokes' kernel (classical Stokes geoid); Stokes' integral using the modified Stokes' kernel created by Wong and Gore (Stokes/Wong geoid); Stokes' integral using the Meissl's modified Stokes' kernel (Stokes-Meissl geoid); Stokes' integral using the Heck and Grüninger modified Stokes' kernel (Stokes/Heck geoid); Stokes' integral using window technique (Window geoid).

The GPS-GEOID is used to compare all the computed geoids.

The absolute geoid discrepancies between the conventional Stokes geoid and the geoid determined from GPS levelling are presented in Figure 6. These geoid height differences have a standard deviation of 3.0 m, an average of 1.8 m, and a range of −2.8 m to 9.2 m. It can be seen from the figure that, the differences approximately reflect the topography. The values of differences are positive in the western desert where the topographic heights are positive. Also, the values are negative in the Red Sea region as the bathymetric heights are negative. Finally, the contour lines are smooth as the topographic heights in Egypt are rough, not rugged.

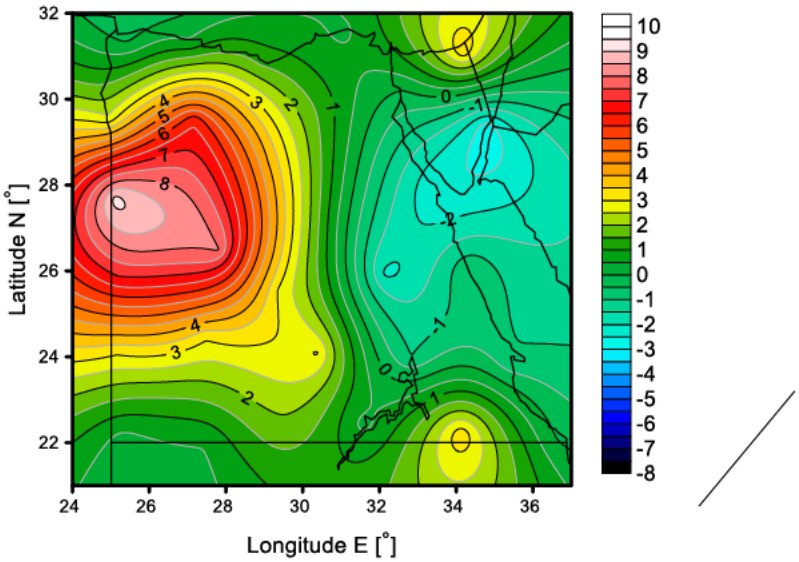

Figure 6 Geoid height discrepancies between original Stokes geoid and GPS-GEOID.

As previously mentioned, the optimal capsize $\psi_\circ$ for the case of Meissl modified kernel can be estimated empirically. This is accomplished by contrasting the GPS/levelling geoid to the computed Stokes-Meissl geoid. The statistical results of the empirical Stokes- Meissl geoid's capsize $\psi_\circ$ are presented in Table 2. It demonstrates that the optimal capsize with the minimum standard deviation of the variations to the GPS-levelling computed geoid is given by $\psi_\circ = 1.5^\circ$.

Figure 7 illustrates the geoid undulations discrepancies between the geoid estimated from GPS-levelling and the Stokes-Meissl geoid with capsize $\psi_\circ = 1.5^\circ$). These differences vary between −5.67 m and 4.66 m, with an average of −0.31 m and a standard deviation of 2.47 m. Figure 7

exhibits a higher quality polynomial structure for the differences compared to the Stokes geoid scenario (compare Figs. 6 and 7). Meissl-modified-Stokes-kernel provides the least range of absolute geoid discrepancies compared to the other modified kernels.

Table 2: The empirical evaluation's statistics of the cap- size ψ◦ for the Meissl-geoid

Capsize	Discrepancies to GPS-levelling geoid			
	min	max	average	std
	m	m	m	m
$\psi_\circ = 1.0^\circ$	−6.31	4.09	−0.40	2.47
$\psi_\circ = 1.5^\circ$	−5.67	4.66	−0.31	2.47
$\psi_\circ = 1.7^\circ$	−5.44	4.87	−0.27	2.48
$\psi_\circ = 2.0^\circ$	−5.14	5.17	−0.22	2.51
$\psi_\circ = 2.5^\circ$	−4.88	5.57	−0.14	2.57

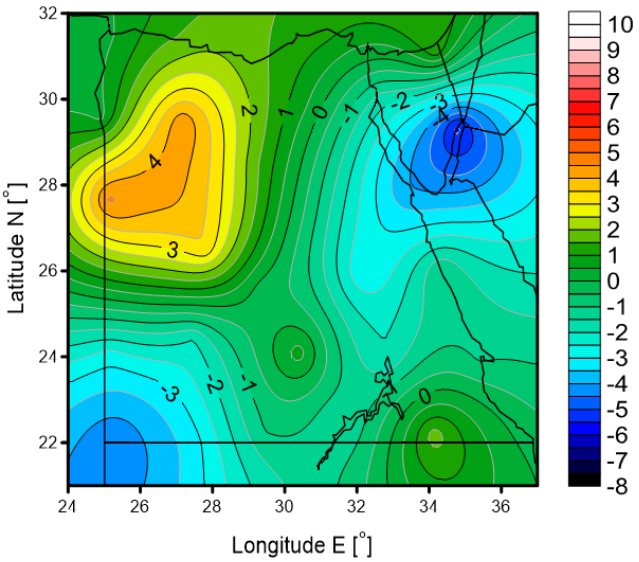

Figure 7 Geoid discrepancies between Stokes-Meissl geoid (capsize ψ◦ = 1.5◦) and geoid from GPS-levelling.

The geoid height discrepancies between the geoid estimated from the window technique and the geoid resulting from GPS-levelling are shown in Figure 8. These differences have a standard deviation of 2.8 m with an average of 0.60 m and a range between −3.4 m and 7.7 m in comparison to the Stokes geoid, the range of geoid differences for the window geoid declines by around 1 m, and the standard deviation declines by around 0.2 m. Indeed, in comparison to the Stokes-geoid, Figure 8 depicts a higher-quality polynomial ordering of the discrepancies.

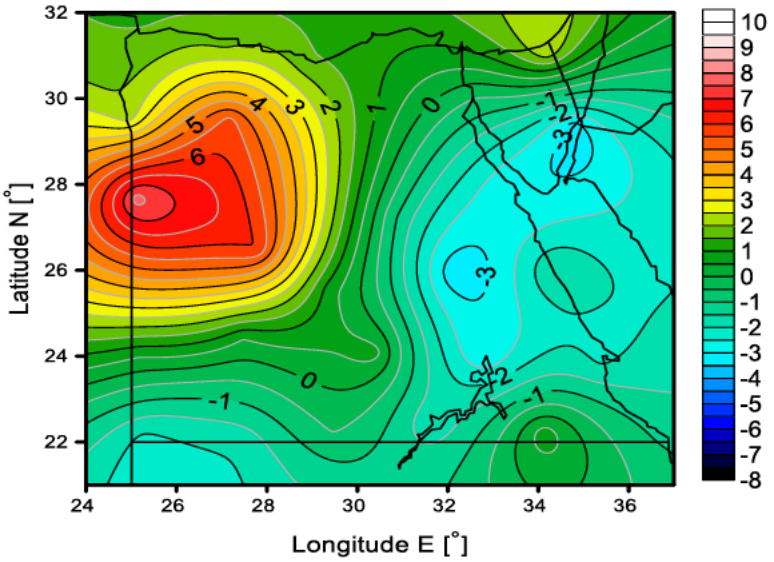

Figure 8 Geoid height differences between geoid form window approach and geoid from GPS-orthometric heights.

The optimal capsize for the Wong and Gore geoid can also be obtained empirically by contrasting the calculated Stokes-Wong geoid with the geoid estimated from GPS-levelling. The numerical tests' statistics for the capsize $\psi_\circ$ for the Wong geoid are presented in Table 3. It demonstrates that $\psi_\circ = 1.0^\circ$ provides the optimal capsize with the minimum standard deviation of the variations to the geoid determined from GPS. Table 3 also demonstrates the degree of modification L corresponding to each value of the capsize $\psi_\circ$ computed using the method described in sec. 5.2.

Table 3: The empirical evaluation's statistics of tests for the different capsizes ψ° for the Stokes-Wong geoid

Capsize	iscrepancies to GPS-levelling geoid			
	L	min	max	average
	—	m	m	m
$(\psi_\circ = 0.5^o)$	111	−7.80	3.27	−0.57
$(\psi = 0.7^o)$	91	−7.61	3.40	−0.53
$(\psi_\circ = 1.0^o)$	63	−6.84	3.86	−0.43
$(\psi = 1.5^o)$	43	−5.68	4.42	−0.26
$(\psi_\circ = 2.0^o)$	32	−5.36	5.38	−0.20

Figure 9 illustrates the absolute geoid discrepancies between the geoid after Wong modification ($\psi_\circ = 1.0^\circ$) and the geoid determined from GPS-levelling. These discrepancies have a standard deviation of 2.56 m with an average of −0.43 m and scope between −6.84 m and 3.86 m. For the Stokes-Wong geoid, the standard deviation drops by around 0.4 m, and the range of differences drops by about 1.3 m in comparison to the Stokes geoid.. A better polynomial ordering for the differences is shown in Figure 9.

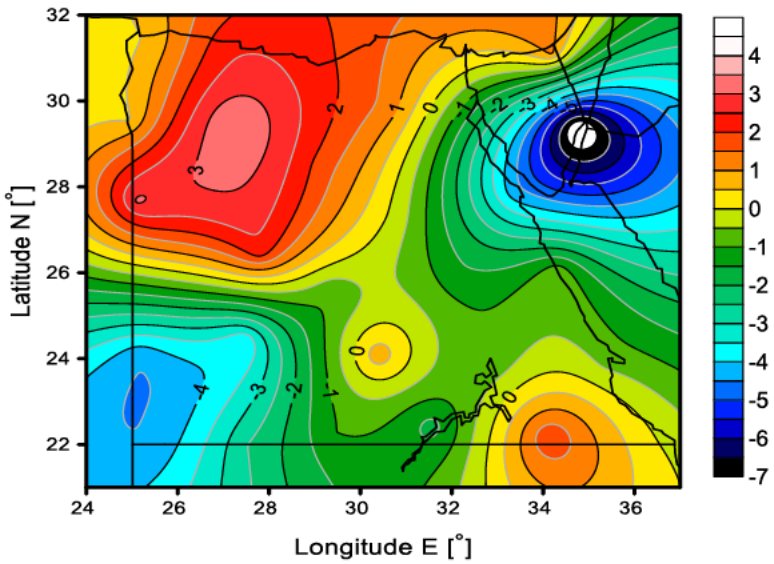

Figure 9 Absolute geoid difference between Stokes/Wong geoid (capsize $\psi_\circ = 1.0^\circ$) and GPS/leveling derived geoid.

For the case of Heck-geoid, to obtain the ideal cap- size $\psi_\circ$ numerically, the estimated Stokes-Heck geoid to the geoid determined from GPS-levelling are compared. The empirical tests' statistics for the Stokes-Heck geoids capsize $\psi_\circ$ are presented in Table 4. It demonstrates that the ideal capsize with the minimum standard deviation of the absolute differences from the geoid determined by GPS is given by $\psi_\circ = 2.0^\circ$ Additionally, Table 4 also shows the degree of modification k corresponding to each value of the capsize $\psi_\circ$ computed using the approach described in sec 5.3.

Table 4: The empirical tests' statistics for the capsize $\psi_\circ$ for the Stokes-Heck geoid.

Capsize	Discrepancies to GPS-levelling geoid			
	k	min	max	average
	—	m	m	m
$(\psi_\circ = 1.0^o)$	94	−7.72	3.38	−0.61
$(\psi = 1.5^o)$	77	−7.34	3.60	−0.55
$(\psi_\circ = 2.0^o)$	58	−5.79	4.57	−0.32
$(\psi = 2.5^o)$	49	−7.28	3.88	−0.48
$(\psi_\circ = 3.0^o)$	39	−7.37	3.92	−0.48

Figure 10 demonstrates discrepancies between the Heck-geoid (capsize equals $\psi_\circ = 2.0^\circ$) and the geoid determined for GPS-orthometric heights. These absolute geoid differences have a standard deviation of 2.46 m, an average of −0.32, and a range between −5.79 m and 4.57 m. In comparison to the Stokes geoid, the Stokes- Heck geoid's range of geoid differences is reduced by around 0.9 m, and its standard deviation is reduced by a round 0.5 m. In comparison to the Stokes geoid scenario, Fig. 10 illustrates the absolute geoid differences with a better polynomial structure.

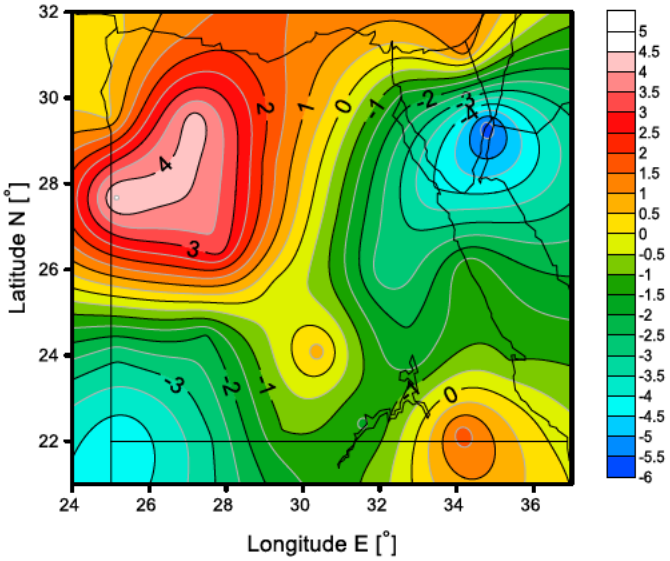

Figure 10 Absolute geoid discrepancies between Stokes-Heck geoid (capsize ψ◦ = 2.0◦) and GPS-geoid.

As shown in Figures 6 to 10, the outcomes of using the window technique or Stokes' integral with modified Stokes kernels are superior to those of using the classical kernel. With the window technique and with all approaches employing modified Stokes' kernels, similar results are achieved. Using the adapted Stokes' kernel after Meissl yields a somewhat better polynomial structure (Fig. 7).

Table 5: Statistics of the discrepancies between the estimated geoids from anomalies and the geoid determined from GPS-levelling.

Geoid strategy	Statistical parameters			
	min	max	average	std
	m	m	m	m
un-modified Stokes	−2.80	9.20	1.80	3.00
Meissl approach	−5.67	4.66	−0.31	2.47
Wong approach	−7.80	3.51	−0.47	2.59
Heck approach	−5.79	4.57	−0.32	2.46
window technique	−3.40	7.70	0.60	2.80

Table 5 displays the statistics of the discrepancies between the determined geoids within the scope of the current study and the geoid estimated from GPS-levelling. It demonstrates that there are significant variations between the geoid from GPS-levelling and the unaltered Stokes geoid. This supports the earlier claim that RRM implies the incorrect gathering of gradational field wave lengths when utilizing the classical, unmodified Stokes kernel. Additionally, Table 5 demonstrates that the window approach or un-modified Stokes kernel produces greater differences from the GPS-GEOID (in terms of the square root of the variance of the differences).

Finally, a polynomial regression surface of the fourth order has also been removed from the fitting of the calculated geoids within the current inquiry for the sake of comparison. Following the

removal of the polynomial surface, Table 6 displays the residuals at the 30 GPS stations. As a result of using all GPS stations throughout the fitting procedure, Table 6 illustrates the internal accuracy of the fitted geoids.

Table 6: The remaining residuals' statistics at the 30 GPS stations after removing a 4th-degree polynomial surface (internal geoid precision)

Geoid strategy	Statistical parameter			
	min	max	average	std
	m	m	m	m
un-modified Stokes	−2.80	2.90	0.0	0.89
Meissl approach	−2.40	2.52	0.0	0.65
Wong approach	−2.42	2.54	0.0	0.67
Heck approach	−2.39	2.51	0.0	0.65
window technique	−2.45	2.50	0.0	0.72

10. Conclusion

The synthesis of the various wavelengths of the Earth's gravitational field cannot be handled properly by the Stokes technique using a conventional Stokes kernel within RRM. New approaches or modifications to the kernel should be provided. Three modifications of the Stokes kernel have been examined, which are Stokes' integral using Meissl, Wong, and Gore and Heck and Grüninger modifications kernel. In addition, the window technique has been formulated. The results proved that the merging of the geoid wavelengths can be handled properly using the previously mentioned techniques within the RRM. Stokes' integral using modified Stokes, as well as using the window approach, gives better variation to geoid derived from GPS-levelling.

Firstly, from our computations, it can be concluded that the conventional remove-restore technique should not be applied for the determination of gravity anomalies and geoid determination. Therefore, for precise geoid determination, either remove- restore technique must be modified or the classical Stokes Kernel must be modified.

The numerical computation indicated that the gravity anomalies that came out from the window approach are the finest (have the smallest standard deviation), unbiased, and have the minimum range. Therefore, the final anomalies resulting from the window approach are best suited for geodetic and geophysical uses due to this characteristic. It is worth mentioning that as the differences between all tested modified Stokes' kernels and the window approach are small, one may recommend using the WRRM, proposed by [18] since it provides the smoothest reduced-gravity-anomalies and its theory is rather unambiguous.

Conflict of Interest

The authors state that none of their known conflicting financial interests or personal connections could have had an impact on the work that was published in this book.

Acknowledgment

We are very grateful for the careful reviews of the anonymous reviewers. Indeed, it helped us to reconsider some essentials which led to some additional test results and a considerable (major) improvement of the paper. Also, we are grateful to the editor-in-chief.

References

1. Abd-Elmotaal HA, Seitz K, Kühtreiber N, Heck B (2019) AFRgeo_v1.0: a geoid model for Africa. KIT Scientific Working Papers 125. https://doi.org/10.5445/IR/1000097013
2. Novák P, Vaníček P, Véronneau M, Holmes SA, Featherstone WE (2001) On the accuracy of modified Stokes's integration in high-frequency gravimetric geoid determination. J. Geod., 74, 644-654.
3. Sjöberg LE, Hunegnaw A (2000) Some modifications of Stokes' formula that account for truncation and potential coefficient errors. J Geod 74:232–238.
4. Sjöberg LE (2003a) A computational scheme to model the geoid by the modified Stokes formula without gravity reactions. J Geod 77:423–432.
5. Sjöberg LE (2003b) A general model for modifying Stokes formula and its least-squares solution. J Geod 77:459–464.
6. Featherstone WE (1999) A comparison of gravimetric geoid models over western Australia, computed using modified forms of Stokes' integral. Journal of the Royal Society of Western Australia 82:137–145.
7. Abd-Elmotaal HA, Ku¨htreiber N (2007) Modified Stokes ker- nel versus window technique: Comparison of optimum combination of gravity field wavelengths in geoid computation.
8. Sjöberg LE (2004) A spherical harmonic representation of the ellipsoidal correction to the modified Stokes formula. J Geod 78:180–186.
9. Abd-Elmotaal HA (2007) Reference geopotential models tailored to the Egyptian gravity field. Boll Geod Sci Affini 66(3):129–144.
10. Silva MA, Blitzkow D, Lobianco MCB (2002) A case study of different modified kernel applications in quasi-geoid determination. Proceedings of the 3rd Meeting of the International Gravity and Geoid Commission, Thessaloniki, Greece, August 26-30, pp 138–143.
11. Featherstone WE (2003) Software for computing five existing types of deterministically modified integration kernel for gravimetric geoid determination. Comput Geosci 29:183– 193.
12. Novák P, Vaníček P, V´eronneau M, Holmes S, Featherstone WE (2001) On the accuracy of modified Stokes integration in high-frequency gravimetric geoid determination. J Geod 74:644–654.
13. Abd-Elmotaal HA, Ku¨htreiber N (2008) An attempt towards an optimum combination of gravity field wavelengths in geoid computation. Observing our Changing Earth, J IAGS 133:203–209, DOI 10.1007/978-3-540-85426-5 24.
14. Pail R, Bruinsma S, Migliaccio F, Förste C, Goiginger H, Schuh W, Höck E, Reguzzoni M, Brockmann J, Abrikosov O, Veicherts M, Fecher T, Mayrhofer R, Krasbutter I, Sansó F, Tscherning C (2011) First GOCE gravity field models derived by three different approaches. J Geod 85(11):819–843, DOI 10.1007/s00190-011-0467-x.
15. Abd-Elmotaal HA, Makhloof A (2013) Gross-errors detection in the shipborne gravity data set for Africa. Presented at Geodetic Week, Essen, Germany, October 8-10, 2013 2013.

16. Abd-Elmotaal HA and Makhloof A (2013) Comparison of Recent Geopotential Models for the Recovery of the Gravity Field in Egypt. Geodetic week conference 8-11 Oktober 2013.
17. Abd-Elmotaal HA, Abd-Elbaky M, Ashry M (2013) 30 meters digital height model for. VIII Hotine-Marussi Symposium, Rome, Italy, June 17–22, 2013.
18. Abd-Elmotaal HA, Kühtreiber N (2003) Geoid determination using adapted reference field, seismic Moho depths, and variable density contrast. J Geod 77(1-2):77–85.
19. Abd-Elmotaal HA, Ashry M (2013) The 3″ digital height model for Egypt - egh13. 8th International Conference of Applied Geophysics, Cairo, Egypt, February 25-26, 2013.
20. Forsberg R (1993) Modelling the fine structure of the geoid: methods, data requirements, and some results. Surv Geo- phys 14:403–418.
21. Sansó F (1997) Lecture notes: Int school for the determination and use of the geoid. Int Geoid Service, DIIAR-Politecnico diMilano, Milan.
22. Rapp R, Rummel R (1975) Methods for the computation of detailed geoids and their accuracy. Ohio State University, Department of Geodetic Science and Surveying, Rep 233.
23. Vincent S, Marsh J (1974) Gravimetric global geoid. In: Veis G (ed) Proc Int Symp on the use of artificial satellites for geodesy and geodynamics, Athens.
24. Heiskanen WA, Moritz H (1967) Physical Geodesy. Freeman, San Francisco.
25. Molodenesky MS, Eremeev VF, Yurkina MI (1962) Meth- odes for the study of the external gravitational field and figure of the Earth. Israel Program for Scientific Translations, Jerusalem.
26. Meissl P (1971) Preparation for the numerical evaluation of second order Molodensky-type formulas. Ohio State University, Department of Geodetic Science and Surveying, Rep 163.
27. Wong L, Gore R (1969) Accuracy of geoid heights from modified Stokes kernels. Geophys J R Astr Soc 18(1):81–91.
28. Vaníček P, Featherstone WE (1998) Performance of three types of Stokes' kernel in the combined solution for the geoid. J Geod 72:684–697.
29. Featherstone WE, Evans JD, Olliver JG (1998) A Meissl- modified Vaníček and Kleusberg kernel to reduce the truncation error in geoid computations. J Geod 72:154–160.
30. Grombein T, Seitz K (2010) Die stokes-funktion und modifizierte kernfunktionen. Vernetzt und ausgeglichen: Festschrift zur Verabschiedung von Prof Dr-Ing habil Dr-Ing Eh Günter Schmitt p 89.
31. Colombo O (1981) Numerical methods for harmonic analysis on the sphere. Ohio State University, Department of Geodetic Science and Surveying, Rep 310.
32. Heck B, Seitz K (1991) Harmonische Analyse. Technical Report, Geodetic Institute, University of Karlsruhe.
33. Abd-Elmotaal HA (2004) An efficient technique for harmonic analysis on a spheroid (ellipsoid and sphere). VGI 3(4):126–135.
34. Heck B, Gru¨ninger W (1987) Modification of Stokes's integral formula by combining two classical approaches. Proceedings of the XIX General Assembly of the IUGG, Vancouver, Canada 2:309–337.
35. Featherstone W, Kirby J, Hirt C, Filmer M, Claessens S, Brown N, Hu G, Johnston G (2011) The AUSGeoid09 model of the Australian height datum. J Geod 85(3):133–150.
36. Claessens SJ, Hirt C, Amos M, Featherstone W, Kirby J (2011) The NZGEOID09 model of New Zealand. Surv Rev 43(319):2–15.

37. Hanafy M (1987) Gravity field data reduction using height, density, and Moho information. Ph.D. Dissertation, Institute of Theoretical Geodesy, Graz University of Technology.
38. Sünkel H (1985) An isostatic earth model. Ohio State University, Department of Geodetic Science and Surveying, Rep 367.
39. Rummel R, Rapp R, Sünkel H, Tscherning C (1988) Comparison of global topographic/isostatic models to the Earth's observed gravity field. Ohio State University, Department of Geodetic Science and Surveying, Rep 388.
40. Abd-Elmotaal HA (2008) Gravimetric geoid for Egypt using high-degree tailored reference geopotential model. NRIAG Journal of Geophysics, Special Issue pp 507–531.
41. Abd-Elmotaal HA (2014) Egyptian geoid using ultra high-degree tailored geopotential model. In: Proceedings of the XXV FIG Congress, Kuala Lumpur, Malaysia, June 16-21, 2014, URL http://www.fig.net/pub/fig2014/papers/ts02a/TS02.
42. Förste C, Bruinsma S, Flechtner F, Marty J, Lemoine J, Dahle C, Abrikosov O, Neumayer H, Biancale R, Barthelmes F, Balmino G (2012) A new release of eigen-6c. American Geophysical Union, Fall Meeting, San Francisco, USA, December 3-7, 2012.

مقارنة الطرق المختلفة للجمع بين الأطوال الموجية لمجال الجاذبية

الملخص العربى

في سياق تقنية الحذف والاضافة يسعى هذا البحث إلى تحديد أفضل مزيج من الأطوال الموجية لمجال الجاذبية لحساب الجيود في مصر. توجد عادة عدد من الطرق لدمج هذه الاطوال الموجية. لقد تم اقترح البيانات الأرضية مع النماذج المرجعية لجاذبية الأرض باستخدام نموذج ستوكس بعد تعديله بطرق مختلفة. ايضا قد تم معالجة الاعتبار المزدوج للكتل الطبوغرافية والتعويضية داخل النافذة المحسوبة بشكل صحيح من خلال تقنية تسمى تقني النافذة للحذف والاضافة. في إطار حساب الجيود، تم إجراء مقارنة شاملة لدالة ستوكس المعدلة مع الأساليب وتقنيات النوافذ المختلفة. تم إجراء المقارنة على مستويين منفصلين: حيود الجاذبية بعد الاختزال إلى مجسم أرضي باتباع خطوة الإزالة الصحيحة والارتفاعات الجيودي المحددة فيما يتعلق بالمجسم الأرضي المحدد من خلال تسوية نظام تحديد المواقع العالمي (GPS-GEOID). اولاً من حساباتنا، يمكن أن نستنتج أن تقنية الإزالة والاستعادة التقليدية لا ينبغي تطبيقها لتحديد حيود الجاذبية وتحديد الجيود. كما أظهرت النتائج أن حيود الجاذبية المقدرة باستخدام تقنية النافذة هي مستقلة، والأفضل. ثانيا الجيويد الناتج من نظام تحديد المواقع العالمي (GPS) يحتوي على اختلافات أقل بينه وبين الجيويد المحسوبة باستخدام نواة ستوكس المعدلة بالإضافة إلى الجيويد المحدد باستخدام تقنية النافذة مقارنة بحالة استخدام نواة ستوكس الكلاسيكية غير المعدلة. أخيرًا تعطي نهج النافذة نتائج أفضل تمامًا مقارنةً بطريقة النواة غير المعدلة من ستوكس.